Tbx1 regulates extracellular matrix- and cell-cell interactions in the second heart field.

Daniela Alfano[1*], Alessandra Altomonte[1], Marchesa Bilio[1], and Antonio Baldini[1,2*].

1) CNR Institute of Genetics and Biophysics Adriano Buzzati-Traverso, Via Pietro Castellino 111, 80131 Naples, Italy.

2) Department of Molecular Medicine and Medical Biotechnology, University of Naples Federico II, Naples 80131, Italy.

* corresponding authors.

Address for correspondence:

Daniela Alfano, PhD
Institute of Genetics and Biophysics, CNR
Via Pietro Castellino, 111
80131 Napoli, Italy
e.mail: daniela.alfano@igb.cnr.it
Tel: +39-0816132409

Or

Antonio Baldini, MD
Institute of Genetics and Biophysics, CNR
Via Pietro Castellino, 111
80131 Napoli, Italy
e.mail: antonio.baldini@unina.it
Tel: +39-0816132219

Short title: TBX1 controls cell-ECM and cell-cell interactions

ABSTRACT

Tbx1, a gene involved in DiGeorge syndrome, is required for efficient incorporation of cardiac progenitors (CPs) of the second heart field (SHF) into the heart. However, the mechanisms by which TBX1 regulates this process are still unclear. Here, we have used two independent models, *in vivo* and *in vitro,* to define the role of TBX1 in establishing morphological and dynamic characteristics of target cells in the mouse. We found that loss of TBX1 impairs cell migration and adhesion *in vitro* and affects the axis extra cellular matrix (ECM)-integrin-focal adhesion in both models. In addition, the ECM-mediated outside-in signalling is disrupted in the absence of TBX1. Furthermore, we found that the epithelial-like layer of the SHF exhibits an apical-lateral adhesion domain containing E-cadherin, beta-catenin, paxillin, and non-muscle myosin II (NMIIB). Interestingly, loss of *Tbx1* affects this adhesion domain and causes loss of polarity and alteration of focal adhesion proteins. We propose that TBX1 is required for condensation of splanchnic mesodermal cells into the epithelial-like layer of the dorsal pericardial wall. In summary, our data identifies TBX1 as an important player in SHF tissue architecture via regulation of ECM-cell and cell-cell interactions.

Keywords: Tbx1, cardiac progenitors, second heart field, extra cellular matrix.

Non-standard abbreviations and Acronyms:
CDH1 E-cadherin
COLI collagen type I
E Embryonic day
ECM extracellular matrix
FA focal adhesion
GFP green fluorescent protein
IF immunofluorescence
NMIIB non-muscle myosin II isoform B (MYH10)
OFT outflow tract
PXN paxillin
PCR polymerase chain reaction
SHF second heart field
TBX1 T-box transcription factor 1
VCL vinculin
WT wild-type

Significance Statement

The 22q11.2 deletion is the second most common known genetic cause of congenital heart disease (CHD) after trisomy 21. *TBX1* gene haploinsufficiency is the main cause of CHD in this condition. Here, *in vivo* and *in vitro* models reveal that TBX1 is a regulator of the extra cellular matrix-integrin-focal adhesion axis, and the outside-in signaling, thus controlling cell dynamics and interactions. We show that in mouse mutants, the tissue architecture of the splanchnic mesoderm and dorsal pericardial wall, a region that includes cardiac progenitors of the second heart field, is disrupted, providing novel insights into the mechanics of cardiac progenitors incorporation into the developing heart.

INTRODUCTION

The heart develops from populations of progenitor cells that are specified as early as gastrulation. In vivo die-labeling and genetic clonal analyses have identified at least two distinct populations, first (FHF) and second (SHF) heart fields (1-5) that originate from *Mesp1*-expressing cells of the primitive streak (6, 7).

The SHF is part of a mesodermal population that gives rise to cardiomyocites as well as other cell types, such as skeletal muscle of the branchiomeric musculature and some populations of endothelial cells. Overall, this multipotent cell population is referred to as the cardiopharyngeal mesoderm (CPM) lineage (8).

CPM/SHF progenitors are specified in the mouse at around E7.5 and are characterized by a complex ontology. They migrate as part of the splanchnic and pharyngeal mesoderm and undergo differentiation into distinct cell types, i.e. cardiomyocytes, skeletal myocytes, endothelial cells, and smooth muscle cells. The cellular and molecular genetic mechanisms by which progenitor cells are directed and sorted into the different cell types and regionalized in the pharyngeal apparatus towards the two heart poles are only now beginning to emerge. Specifically, SHF progenitors destined to contribute to the arterial and venous poles of the heart condense into an epithelial-like monolayer of cells, between E8 and E9.5, that also form the dorsal pericardial wall (DPW). This epithelial sheet is under tension and its cells are gradually incorporated into the two poles of the heart (9). How cells of the splanchnic mesoderm (SpM) become organized and condensed into an epithelial-like sheet is not completely clear. Planar cell polarity (PCP) genes *Dvl2* and *Wnt5a* have been proposed to be part of this process by facilitating the incorporation, by intercalation, of mesenchymal cells into the epithelial sheet of the DPW (10-12). *Tbx1* has been shown to be required for progenitors recruitment to the heart (13, 14) and its loss has been associated with disruption of epithelial polarity of the DPW (15), and reduced tension of the epithelial sheet (9), although the mechanisms by which these phenotypic anomalies occur remain unclear. TBX1 regulates *Wnt5a* expression in the SHF (16), suggesting that at least some of the tissue architectural roles of TBX1 may be operated through the Wnt non canonical/PCP pathways. However, $Wnt5a^{-/-};Tbx1^{-/-}$ embryos have much more severe heart defects than the individual mutants providing genetic evidence that the two genes also have non overlapping functions in heart development (16).

Here, we use two independent models, *in vivo* and *in vitro*, to show that *Tbx1* regulates the extra cellular matrix-integrin-focal adhesion axis, and alters the condensation of mesenchymal splanchnic mesoderm into the epithelial-like layer of the dorsal pericardial wall. We found that TBX1 is required for ECM-intracellular signaling. Finally, we found that the epithelial layer of the SHF has an apical adhesion domain that includes immunoreactivity for E-cadherin, beta-catenin, Paxillin, and actomyosin, and this domain is disrupted in $Tbx1^{-/-}$ embryos.

RESULTS

Tbx1 regulates cell migration, polarization, and adhesion in cultured cells.

To begin to understand whether TBX1 is involved in cell movements, we used a generic 4 hrs. cell migration assay in a chemotactic gradient of serum. For this, we used two independent cell lines that express *Tbx1*: C2C12 undifferentiated myoblast cells and mouse embryonic fibroblasts (MEFs).

For C2C12 cells, we used RNA interference to knock down *Tbx1* expression, while MEFs were obtained from WT, *Tbx1*$^{+/-}$ and *Tbx1*$^{-/-}$ embryos. Results showed that migration was significantly reduced following TBX1 dosage reduction or elimination (Fig. 1A-B and Supplementary Fig. 1A). We also used a two dimensional 24 hrs. assay based on closure of mechanically inflicted wounds in confluent cell monolayers, monitored by time-lapse microscopy. *Tbx1* depletion substantially reduced C2C12 cell migration into the wound area (Fig. 1C); this effect was not due to differences in cell proliferation because we did not find a significant change in cell proliferation in the time window within which the migration assay was performed (Supplementary Fig. 1B). Furthermore, we found that migrating *Tbx1*-depleted (*Tbx1*^{KD}) cells plated on the extracellular matrix (ECM) component Collagen 1 (COLI encoded by the *Col1a1* gene) failed to polarize properly, as they exhibited aberrant repositioning of the Golgi apparatus (Fig. 1D). The number of polarized cells was reduced by 80% in *Tbx1*^{KD} cells compared with control cells. Phalloidin staining revealed that control cells formed lamellipodia at the edge of the wound but *Tbx1*^{KD} cells showed fewer lamellipodial protrusions (Fig. 1D and Supplementary Fig. 2A), indicating that TBX1 is required for the formation of these structures, which produce the driving force for migration. Moreover, immunofluorescence (IF) with an anti alpha-tubulin antibody showed that in control cells the signal is mainly distributed at the leading edge, while in *Tbx1*^{KD} cells the microtubule distribution is more uniform around the cells (Fig. 1E and Supplementary Fig. 2B), confirming a polarization defect.

The migration impairment might be due to defective interactions with the substrate (17). The cell spreading assay in tissue culture is useful to test cell adhesion defects and, in particular, defects regarding the formation and disassembly of initial adhesive cell contacts. C2C12 cells were plated on ECM components COLI, Fibronectin (FN), or Matrigel, or uncoated plastic. After 20 min from seeding, we have evaluated the spread area. We found that *Tbx1*^{KD} C2C12 cells had a significantly reduced spread area and perimeter compared to non-target (NT) siRNA-treated control cells on all substrates, except FN (Fig. 2A). *Tbx1*^{KD} cells appeared rounded and less spread compared to control cells (Fig. 2B). *Tbx1* depletion did not alter significantly the size of cells in suspension (Fig. 2C). After 120 min from plating, however, the spreading of *Tbx1*^{KD} cells was normal, suggesting that there was a delay rather than a block of spreading. *Tbx1* knockdown did not significantly affect cell adhesion to plastic uncoated or coated with COLI or FN (Fig. 2D). Thus, *Tbx1*^{KD} cells adhere to substrate but do not spread properly. Furhermore, we found that the expression of *Itgb1* (encoding integrin beta 1 or ITGB1) was decreased in *Tbx1*^{KD} cells (Fig. 2E) where the protein product was reduced in the membrane and in focal adhesions (FAs), as shown by flow cytometry and IF, respectively (Fig. 2F-H). In addition, *Tbx1*^{KD} cells showed a significant increase of aberrant protrusions (Fig. 2I), a phenotype previously shown to be associated with loss of Focal Adhesion Kinase (FAK) or Paxillin (PXN) (18, 19). Indeed, PXN, which is a major adapter protein of FAs, was down regulated at both mRNA and protein levels in *Tbx1*^{KD} cells (Fig. 3A), consistent with a report showing that *Pxn* is a direct target gene of TBX1, albeit in a different cell line (20). Given these results, we tested for possible FA abnormalities. We analysed control and *Tbx1*^{KD} cells in two different conditions of spreading that stimulate focal complex and adhesion formation (here collectively referred to as FAs): 1) in acute serum-induced spreading, or 2) by plating on ECM (COLI or FN). Results, obtained by PXN or phospho-PXN immunostaining, revealed that *Tbx1*^{KD} cells had a reduced number of FAs/cell compared to control cells, in both conditions (Fig. 3B-C, upper and middle panels and Fig. 3D). Moreover, in *Tbx1*^{KD} cells, the area and perimeter occupied by FAs relative to the total spread area and perimeter of the cell was significantly lower compared to control cells (Fig. 3B-C upper and middle panels). Similarly, vinculin (VCL), which is a membrane-cytoskeletal protein in FA plaques, highlighted elongated fibrillar adhesions over the entire ventral surface of control cells by IF, whereas in *Tbx1*^{KD} cells, the VCL staining was predominantly restricted to shorter plaques and we rarely observed elongated FAs (Fig. 3B, lower panels). Quantitative analysis of VCL IF showed that the number and size of FAs were reduced in *Tbx1*^{KD} cells compared to control cells (Fig. 3C, lower panels).

The ECM-Integrin-FA axis is altered in the SHF of *Tbx1* mutants.

Data obtained with cultured cells point to a broad role of TBX1 in regulating cell dynamic characteristics and shape. We set to validate these findings in vivo, specifically in the SHF, which is the principal target of *Tbx1* during heart development. At E9.5 COLI was expressed in the SpM,

lateral and posterior to the DPW (Fig. 4A) and in the mesenchymal tissue adjacent and abutting to the basal side of the epithelial-like layer of the epithelial-like layer of the SHF (eSHF), where it formed a rudimentary basal lamina, but it was not found laterally or apically to the eSHF cells (Fig. 4C). In *Tbx1*$^{-/-}$ embryos, COLI immunostaining was increased in the SpM and we noted a broader and mislocalized distribution in the eSHF where the collagen fibrils were randomly distributed around the cells, rather than being restricted to a basal lamina (Fig. 4B-D and Supplementary Fig. 3).

ITGB1 was expressed in the anterior SHF (here defined as the anterior half of the dorsal pericardial wall, close to the arterial pole of the heart), but not in the posterior SHF (Fig. 4E); it was principally localized at cell-cell contacts and at the basal side of eSHF cells (Fig. 4E and Supplementary Fig. 4), and to a lesser extent at the apical region. ITGB1 was decreased in *Tbx1*$^{-/-}$ embryos compared to WT embryos (Fig. 4F and Supplementary Fig. 3), consistently with in vitro data (Fig. 2E-F).

Next, we used IF with an antibody for the FA marker PXN and found that it is expressed in the SHF and is predominantly localized in the apical and, to a lesser extent, to the basal side of the eSHF (Fig. 5A); apical and basal distribution was also visible in typical epithelia, such as the pharyngeal endoderm (Fig. 5A). Apical PXN partially overlapped with cell-cell adhesion proteins E-cadherin (CDH1) and beta-catenin (CTNNB1) (Fig. 6A-H and Supplementary Movie 1, Supplementary Movie 2). Specifically, the immunostaining overlap was apical-lateral, at the level of cell-cell junctions (Fig. 6A-H), where tight and adherence junction proteins accumulate. In the eSHF we observed a similar pattern with another FA protein, VCL (Fig. 5C). PXN expression in *Tbx1*$^{-/-}$ embryos was reduced and its apical-lateral distribution could not be detected (Fig. 5B). Likewise, VCL was also reduced (Fig. 5D). Moreover, CDH1 was reduced in *Tbx1*$^{-/-}$ mutants and was very low or undetectable in the posterior-lateral regions of the SHF (Supplementary Fig. 5). The cortical actin staining was altered in *Tbx1*$^{-/-}$ mutants (Fig. 7A-B), suggesting impaired assembly of junctional F-actin networks. The actin-motor non-muscle myosin IIB (NMIIB, a.k.a. MYH10) regulates both actin rearrangements and FAs formation and is required for OFT morphogenesis (21-23). We found that NMIIB predominantly decorates the apical side and, to a lesser extent, the lateral side of eSHF cells, while in *Tbx1*$^{-/-}$ embryos, this specific localization was lost and the protein was randomly spread around the eSHF cells (Fig. 7C-D). The anomalous distribution of NMIIB reinforces the idea that TBX1 supports the ability of the eSHF to undergo morphogenetic changes. ECM-cell and cell-cell interactions are critical for cell orientation and polarization. We used Giantin, a Golgi marker, to assay polarity of eSHF cells. In WT embryos the Golgi apparata are clearly aligned at the apical end of cells (Fig. 7E). However, *Tbx1*$^{-/-}$ embryos exhibited de-localization of the Golgi apparatus in approx. 20% of the eSHF cells (Fig. 7F). The polarization defect was observed predominantly in the anterior eSHF (Fig. 7G).

ECM-integrin-FAs, FA-adherens junction complexes, and intermediate filaments are critical components of the mechanosensing machinery (24-28). The intermediate filament Vimentin (VIM) at E8.5 and E9.5 is expressed mainly in endothelial cells and in the heart muscle, and is not detectable in the DPW (Fig. 7H). However, in *Tbx1*$^{-/-}$ embryos, VIM is strongly upregulated in the SHF as well as its immunostaining was increased in the SpM (Fig. 7I and Supplementary Fig. 6-7).

Overall, these findings show that loss of function of *Tbx1* causes a multifaceted cell phenotype related to ECM-cell and cell-cell interactions.

TBX1 is a positive regulator of ECM-mediated signalling.

The alteration of ECM, integrin, and FA proteins expression and/or distribution in *Tbx1* mutant embryos suggest that TBX1 may regulate ECM-cell signalling. Integrins can signal through the cell membrane in either direction: the extracellular binding activity of integrins is regulated from the inside of the cell (inside-out signalling), while the binding of the ECM elicits signals that are transmitted into the cell (outside-in signalling) (29, 30). To determine the consequences of *Tbx1* silencing on outside-in signalling, we analysed the activation of integrin-stimulated signalling cascades in C2C12 cells following adhesion to ECM proteins COLI and FN. In particular, we tested the principal components of PXN-mediated ECM-dependent signalling: FAK, extracellular-signal regulated kinases (ERK1/2), and Cofilin1 (CFL1). The latter is a critical cortical actin regulator, which severs actin filaments to increase the number of sites for actin polymerization in lamellipodia and is inhibited by adhesion signalling (including PXN-signalling) through phosphorylation of Ser3 (31). ECM engagement induced phosphorylation of FAK, ERK1/2, and CFL1 (Fig. 8A-B and

Supplementary 8A) in control cells plated on COLI or FN for 30 min. In *Tbx1*^{KD} cells, the phosphorylation of PXN (Tyr118), FAK (Tyr397 and Tyr925), CFL1 (Ser3) and ERK1/2 were all strongly reduced (Fig. 8A-B). Consistently, P-ERK expression was also found to be reduced in the eSHF of *Tbx1*$^{-/-}$ embryos (15). The defect of signalling cascade activation was only evident in ECM-plated *Tbx1*^{KD} cells (Supplementary Fig. 8B). These results indicate that TBX1 affects two different aspects of ECM signalling: actin dynamics (CFL1), and cell adhesion (FAK, PXN, ERK).

Cell non-autonomous functions of TBX1 in the SHF.

We reasoned that the loss of *Tbx1* may alter the overall tissue environment by altering ECM-cell and cell-cell interactions. If this is the case, the elimination of *Tbx1* in a small number of cells within the tissue should be insufficient to alter the tissue architecture. To test this, we used E9.5 *Tbx1*$^{mcm/flox}$;*R26R*$^{mT\text{-}mG}$ embryos in which Tamoxifen (TM) induction had activated Cre recombination at E7.5. In these embryos GFP+ cells are *Tbx1* functionally homozygous nulls in a heterozygous mutant background as *Tbx1*^{mcm} is a null allele (13). Because of the low efficiency of this MerCreMer driver, GFP+ cells are relatively rare. We used *Tbx1*$^{mcm/+}$;*R26R*$^{mT\text{-}mG}$ as controls. Results showed that NMIIB staining of GFP+ cells in *Tbx1*$^{mcm/flox}$;*R26R*$^{mT\text{-}mG}$ embryos was indistinguishable from that of the surrounding cells of the same embryos or control embryos (Fig. 9A-B). Similarly, VIM immunostaining was normal in GFP+ cells (Fig. 9C-D and Supplementary Fig. 9). Furthermore, CDH1 distribution appeared homogeneous between GFP+ and surrounding cells (Fig. 9C-D and Supplementary Fig. 9). These findings indicate that the anomalous distribution of NMIIB or the alteration of VIM and CDH1 levels are not cell-autonomous phenotypes, suggesting that they are secondary to broad tissue disorganization or that there is a rescue-by-neighbours effect.

DISCUSSION

In this work we show that *Tbx1*, a gene required for cardiac progenitors contribution to the OFT, part of the RV, and interatrial septum, regulates the ECM-cell interface *in vivo* and in cultured cells. Loss of TBX1 reduces cell migration in *in vitro* assays, and affects cell polarity *in vivo* and *in vitro*. Data converge toward a function of TBX1 as a regulator of the axis ECM-integrin-intracellular signalling, which is central for cell migration, polarity, and mechanosensing. Whether or not splanchnic mesodermal cells autonomously migrate into the epithelial-like sheet of the DPW or, alternatively, they follow a coherent, collective movement, remains unclear. Previous data have shown the presence of a proliferative center in the SpM in a dorsal-medial location of the posterior SHF, and suppression of cell proliferation in this region is sufficient to reduce cell contribution to the anterior and posterior SHF (32, 33). This suggests that the SpM proliferation center is a communal source of progenitors for both poles of the heart. Loss of *Tbx1* reduces cell proliferation in the SpM (34-36) and disrupts the geometry of DPW cells (9). Here we add a further layer of complexity to the functions of *Tbx1* in the SHF by revealing a role in regulating interactions with ECM and neighboring cells. In fact, it cannot be excluded that cell proliferation defects may be the consequence of alteration of those interactions. We found FA proteins PXN and VCL localized at the apical and basal sides of eSHF. The basal localization is consistent with typical FA functions in the interaction with the ECM-integrin-FA-cytoskeleton. However, the apical localization and its extensive overlap with E-cadherin and beta-catenin is consistent with association with actin cytoskeleton at epithelial junctions or cell-cell junctions, as previously described in other systems (18), (37-47). The finding that ITGB1 mostly accumulates at cell-cell contacts in the eSHF suggests the existence of an interaction between integrin- and cadherin-mediated cell adhesion complexes. This adhesion complex might represent an anchor point for intercalating mesenchimal cells undergoing incorporation into the eSHF. We propose that this is a process akin to condensation by which loosely organized mesenchymal cells form tightly adherent, polarized epithelial cell sheets. Condensation is mediated by cadherin in a manner that is mechanistically analogous to integrin-mediated spreading on ECM (48).

At the apical/lateral region of the eSHF we also found a contractile protein, NMIIB/MYH10, a non-muscle myosin that has a role in maintaining cortical tension and cell shape control, and is required for heart development (21, 23, 49, 50), although its specific role in the SHF has not been determined. The consequences of NMIIB mislocalization caused by loss of TBX1 are unclear. Recent data show that disruption of the actomyosin machinery using a ROCK inhibitor does not affect

epithelial tension in the SHF, leading the authors to suggest that the major role of actomyosin in this tissue may be to prevent cell distortion secondary to tension (9).

Our *in vivo* mosaic data indicate that at least some of the TBX1 functions in the SHF are non-cell autonomous, consistent with previously reported chimera analyses showing that individual *Tbx1*$^{-/-}$ cells in a WT background are able to contribute to the OFT (13). These findings indirectly support a critical contribution of the ECM to the pathogenesis of phenotypic abnormalities and predict that these abnormalities may arise only if there is a critical number of mutant SHF cells.

Overall, our data indicate that *Tbx1* has broad effects on cell adhesion, morphology, and dynamics *in vitro* and *in vivo*. We found that in the eSHF, PXN, VCL, E-cadherin, F-actin and NMIIB are localized at the apical-lateral region of the monolayer of cells, possibly assembling an actomyosin apparatus that provides, through cortical signaling, cohesiveness among the epithelial-like cells. The localization of most of these proteins and the polarity of eSHF cells is severely altered in mutant embryos, thus compromising the cohesiveness of the cell layer and explaining the previously observed cell roundness and protrusion phenotype (15). The loss of polarity and cohesiveness should also explain the loss of tension within the SHF (9) and the reduced contribution of SHF cells to the heart in these mutants (see model in Fig. 10).

MATERIALS AND METHODS

Mouse lines

The mouse lines *Tbx1*$^{lacZ/+}$ (null allele, here referred to as *Tbx1*$^{-/+}$) (51), *Tbx1*$^{mcm/+}$ (null allele with Tamoxifen-inducible Cre knock in) (13), and *Tbx1*$^{flox/+}$ (conditional floxed allele) (13) were maintained in a clean facility in a C57Bl/6N background. All mouse lines utilized here are available through public repositories: *Rosa*$^{mT/mG}$, The Jackson Laboratory stock N: 007576, *Tbx1*^{mcm}, EMMA repository EM:02404, *Tbx1*$^{flox/flox}$, EMMA repository EM:02135, *Tbx1*^{Lacz}, EMMA repository EM:02137. Genotyping was carried out according to instructions provided by the original reports. The developmental stage of embryos was evaluated by considering the morning of vaginal plug as embryonic (E) day 0.5, and by counting somites of embryos. Embryos were collected at E8.5 and E9.5. To induce nuclear translocation of the MerCreMer fusion protein encoded by the *Tbx1*^{mcm} allele, pregnant mice were intraperitoneally injected twice with Tamoxifen (75 mg/kg body weight) in the morning and afternoon of E7.5. Animal studies were carried out according to the animal protocol 257/2015-PR (licensed to the AB lab) reviewed by the Italian Istituto Superiore di Sanità and approved by the Italian Ministero della Salute, according to Italian regulations.

Cell culture and transfections

Mouse C2C12 undifferentiated myoblast cells obtained from the ATCC (catalog CRL-1772) were cultured in Dulbecco's modified Eagle's medium (DMEM, Invitrogen) supplemented with 10% FBS and L-glutamine (300 µg/ml), and were free of mycoplasma. Primary mouse embryonic fibroblasts (MEFs) were isolated from *Tbx1*$^{+/-}$, *Tbx1*$^{-/-}$, and wild-type embryos at E13.5. To this end, the internal organs, head, tail and limbs were removed. Cells were cultured in Dulbecco's modified Eagle's medium with 20% FBS and 1% NEAA, and used for a maximum of 3 passages. Cells were incubated at 37°C in 5% CO_2. For siRNA transfection, cells were seeded at 1.2×10^5 per well in six-well plates and transfected with a pool of Silencer Select Pre-Designed *Tbx1* SiRNA (Life Technology) (final concentration 50 nmol/L) in antibiotic-free medium using Lipofectamine RNAiMAX Reagent (Life Technology) according to the manufacturer's instructions. 48hrs after siRNA transfection, cells were collected and processed for further analysis.

Immunoblotting

Cells were harvested in lysis buffer (50 mmol/L Tris-HCl pH 7.6, 2 mmol/L EDTA, 150 mmol/L NaCl, 0.5% Triton X-100) supplemented with 1 mM phenylmethylsulphonyl fluoride and 1× complete mini EDTA-free protease inhibitor and PhosSTOP phosphatase inhibitor (Roche). Debris was removed by centrifugation at 10,000 *g* for 20 min at 4°C, and protein content was assessed by a Bradford protein assay. Nuclear proteins were extracted as described previously (18). Proteins were separated by SDS-PAGE and transferred to Immobilon-P PVDF membranes (Biorad). Membranes were subsequently incubated for 1 hour at room temperature in TBST buffer [125 mmol/L Tris-HCl (pH 8.0), 625 mmol/L NaCl, 0.1% Tween 20] containing 5% BSA and further incubated at 4°C for 16

hours with primary antibodies (listed in Table 1). Secondary HRP-conjugated mouse and rabbit (GE Healthcare) or rat (Dako) antibodies were used at a dilution of 1:5000. Membranes were developed using the enhanced chemiluminescence system (GE Healthcare). X-ray films were scanned and processed using ImageJ software for densitometric analysis.

Migration assay

Transwell filters coated with 0.1% gelatin (diluted in PBS) with a PET membrane with 8 μm pores (BD Biosciences) were rehydrated for 2 hrs at 37°C in medium without supplements. Transfected cells were washed once in PBS, and 10^5 cells were seeded into the upper chamber of the Transwells in serum-free medium containing 0.1% BSA. Medium containing 10% FBS or 0.1% BSA was added to the bottom chamber as a chemoattractant. Control wells without FBS were included to assess random migration. Cells were allowed to migrate for 4 hrs at 37°C, in 5% CO_2. The cells on the bottom part of the membrane were fixed in methanol containing 0.1% Crystal Violet. Ten separate bright-field images were randomly acquired of each Transwell filter using a Leica DMI6000 microscope with a Plan APO 10×objective (Leica Microsystems). The cells in each image were counted and analysed in comparison with control-transfected cells. Migration in the absence of FBS (random migration) was taken as 100% for each siRNA treatment, to control for variations in final cell number. For scratch wound assays cells were seeded 24 hrs after transfection in 24-well plates at confluency in growth medium; the confluent monolayer was wounded after 24 hrs by scraping with a pipette tip and then imaged by time-lapse microscopy. A phase-contrast image was acquired every 10 minutes for 18 hrs on a fully motorized Leica DMI6000 microscope with a Plan APO 10× objective. The area occupied by cells in scratch wounds was determined from time-lapse movie images taken at different time after wounding, using ImageJ analysis software. For polarity analysis, cell were plated at confluency on coverslip coated with Collagen I, wounded and fixed 4–6 hrs after wounding for anti-giantin immunostaining.

Cell adhesion and spreading

Flat-bottom 96-well microtiter plates were coated with 10 μg/ml Collagen I (Sigma-Aldrich), 5 μg/ml Fibronectin (Roche), 100 μg/ml Matrigel (BD Biosciences) or 1% heat-denatured BSA in PBS (uncoated plastic) as a negative control, and incubated overnight at 4°C. Plates were then blocked for 1 hour at room temperature with 1% heat-denatured BSA in PBS. Cells were harvested using trypsin and allowed to recover for 1 hr at 37°C, then washed three times in PBS. 10^5 cells were plated in each coated well and incubated for 1 hr at 37°C. Then, culture plates were washed with phosphate-buffered saline (PBS). Attached cells were fixed with 4% paraformaldehyde in PBS for 10 minutes. Cells were finally stained with 0.5% Crystal Violet in 20% methanol. The stain was eluted using 0.1 M sodium citrate in 50% ethanol, pH 4.2, and the absorbance at 595 nm was measured in a spectrophotometer. Alternatively, cells were fixed with 4% paraformaldehyde and counted under the microscope to corroborate the plate reader results. For cell spread area measurements, cells were allowed to spread on the indicated substrates for 20 min and fixed with paraformaldehyde without washing. Cells were then stained for F-actin, and area and perimeter quantified with ImageJ software.

Flow Citometry analysis

For analysis of surface-β1 integrin levels, cells were scraped into PBS, fixed in 4% PFA–PBS for 30 min on ice and fixed with 4% paraformaldehyde; then cells were blocked in 5% BSA–PBS for 30 min on ice. Cells were then incubated with 10 μg/ml anti-integrin β1 for 1 hr on ice. Purified immunoglobulin was used as a negative control. The cells were then washed and incubated with a fluorescein isothiocyanate-labelled goat anti-rat IgG for 30 min at 4°C. Finally, the cells were washed and analysed by flow cytometry using a FACSCanto (Becton Dickinson).

Immunofluorescence and confocal microscopy

Cells were fixed with 4% paraformaldehyde, permeabilized with 0.2% Triton X-100 in PBS, and blocked with 1% BSA in PBS. After incubation with primary antibodies (listed in Table 2), cells were incubated (1hr, RT) with the appropriate secondary antibodies (Alexa Fluor 488, 594; 1:400; Molecular Probes) and, when indicated, with Alexa fluor phalloidin (wavelength 480 nm; Invitrogen)

for F-actin visualization; DAPI was used for nuclear staining. Confocal images were acquired with an inverted confocal microscope (Nikon A1) using 63× (1.4 NA) objective lenses. Images were from cells fixed 48 hrs after transfection unless indicated differently.

FAs size analysis

A pipeline of Cell Profiler software (52) was used to quantify focal adhesions/complexes (number and size) from images of cells stained with anti-paxillin, anti-phospho-paxillin or anti-vinculin antibodies. Cells were either serum starved and stimulated to spread onto ECM-coated coverslips or grown in medium containing 10% FBS on glass coverslips. More than 100 FAs from two different experiments were analysed.

Histology and Immunofluorescence

E9.5 (23-25 somites) mouse embryos were fixed in 4% PFA and embedded in OCT. 10μm sagittal or transverse cryosections and subjected to immunofluorescence using primary antibodies listed in Table 2), and secondary antibodies Alexa fluor 488 (or 594 or 647) Goat anti-rabbit (or anti-mouse or anti-rat) IgG (H+L) (Life Technologies, 1:400). Immunofluorescence experiments were imaged using a NIKON A1 confocal microscope. We tested at least 3 embryos per antibody per genotype.

RNA extraction, cDNA synthesis, and quantitative RT-PCR

RNA was extracted from C2C12 cells using TRI-Reagent (Ambion/Applied Biosystems) according to the manufacturer's protocol. Extracted RNA was treated with DNA-free Kit (Ambion/Applied Biosystems). cDNA was synthesized from 1 μg total RNA (normalized via UV spectroscopy) using the High Capacity cDNA Reverse Transcription Kit, according to the manufacturer's instructions (Applied Biosystems). Target cDNA levels were compared by Q-RT-PCR in 20-μl reactions containing 1× SYBR green (FastStart Universal SYBR Green Master (Rox), Roche), 0.2 μmol/L of each primer. Primers were as follows: for *Tbx1* amplification, forward primer 5'-CTGACCAATAACCTGCTGGATGA-3' and reverse primer 5'-GGCTGATATCTGTGCATGGAGTT-3'; for *Pxn* amplification, forward primer 5'-GCTGCTGCTTCTGCTTCATC-3' and reverse primer 5'- GTGGGTCCTCATTGGTCTGG-3'; for *Rpl13a* amplification, forward primer 5'-CCCTCCACCCTATGACAAGA-3' and reverse primer 5'-CTGCCTGTTTCCGTAACCTC-3'. Results were normalized against *Rpl13a* and compared by relative expression and the delta-delta-cycle threshold method for fold change calculations with the StepOne v2.3 software (Applied Biosystems).

Statistical analysis

Statistical significance was determined by a two-tailed paired Student's t-test. P-values <0.05 were considered as statistically significant. Error bars represent s.d.

Data availability

All the data used in this work are shown in the Figures and in the Supplementary information. All other data supporting the findings of this study are available from the corresponding authors on reasonable request.

ACKNOWLEDGEMENTS

We thank Maddy Parsons for critical reading of the manuscript, and Rosa Ferrentino for excellent technical assistance. We acknowledge the support of the Mouse Facility, Integrated Microscopy, and FACS Facility of IGB-CNR.

Source and Funding

This work was funded in part by grants from the Telethon Foundation (GGP14211), AIRC (IG-17529), and Fondation Leducq (TNE 15CVD01) to AB.

Disclosures
None

REFERENCES

1. Meilhac SM, *et al.* (2003) A retrospective clonal analysis of the myocardium reveals two phases of clonal growth in the developing mouse heart. *Development* **130**(16):3877-3889.
2. Buckingham M, Meilhac S, & Zaffran S (2005) Building the mammalian heart from two sources of myocardial cells. *Nat Rev Genet* **6**(11):826-835.
3. Meilhac SM, Esner M, Kelly RG, Nicolas J-F, & Buckingham ME (2004) The Clonal Origin of Myocardial Cells in Different Regions of the Embryonic Mouse Heart. *Dev Cell* **6**(5):685-698.
4. Zaffran S, Kelly RG, Meilhac SM, Buckingham ME, & Brown NA (2004) Right ventricular myocardium derives from the anterior heart field. *Circ Res* **95**(3):261-268.
5. Vincent SD & Buckingham ME (2010) How to make a heart: the origin and regulation of cardiac progenitor cells. *Curr Top Dev Biol* **90**:1-41.
6. Lescroart F, *et al.* (2014) Early lineage restriction in temporally distinct populations of Mesp1 progenitors during mammalian heart development. *Nat Cell Biol* **16**(9):829-840.
7. Devine WP, Wythe JD, George M, Koshiba-Takeuchi K, & Bruneau BG (2014) Early patterning and specification of cardiac progenitors in gastrulating mesoderm. *Elife* **3**:e03848.
8. Diogo R, *et al.* (2015) A new heart for a new head in vertebrate cardiopharyngeal evolution. *Nature* **520**(7548):466-473.
9. Francou A, De Bono C, & Kelly RG (2017) Epithelial tension in the second heart field promotes mouse heart tube elongation. *Nat Commun* **8**:14770.
10. Sinha T, Wang B, Evans S, Wynshaw-Boris A, & Wang J (2012) Disheveled mediated planar cell polarity signaling is required in the second heart field lineage for outflow tract morphogenesis. *Dev Biol* **370**(1):135-144.
11. Sinha T, *et al.* (2015) Loss of Wnt5a disrupts second heart field cell deployment and may contribute to OFT malformations in DiGeorge syndrome. *Hum Mol Genet* **24**(6):1704-1716.
12. Li D, *et al.* (2016) Spatial regulation of cell cohesion by Wnt5a during second heart field progenitor deployment. *Dev Biol* **412**(1):18-31.
13. Xu H, *et al.* (2004) Tbx1 has a dual role in the morphogenesis of the cardiac outflow tract. *Development* **131**(13):3217-3227.
14. Rana MS, *et al.* (2014) Tbx1 coordinates addition of posterior second heart field progenitor cells to the arterial and venous poles of the heart. *Circ Res* **115**(9):790-799.
15. Francou A, Saint-Michel E, Mesbah K, & Kelly RG (2014) TBX1 regulates epithelial polarity and dynamic basal filopodia in the second heart field. *Development* **141**(22):4320-4331.
16. Chen L, *et al.* (2012) Transcriptional control in cardiac progenitors: Tbx1 interacts with the BAF chromatin remodeling complex and regulates Wnt5a. *PLoS Genet* **8**(3):e1002571.
17. Ridley AJ, *et al.* (2003) Cell migration: integrating signals from front to back. *Science* **302**(5651):1704-1709.
18. Yano H, *et al.* (2004) Roles played by a subset of integrin signaling molecules in cadherin-based cell-cell adhesion. *J Cell Biol* **166**(2):283-295.
19. Owen KA, *et al.* (2007) Regulation of lamellipodial persistence, adhesion turnover, and motility in macrophages by focal adhesion kinase. *J Cell Biol* **179**(6):1275-1287.
20. Fulcoli FG, *et al.* (2016) Rebalancing gene haploinsufficiency in vivo by targeting chromatin. *Nat Commun* **7**:11688.
21. Ma X & Adelstein RS (2012) In vivo studies on nonmuscle myosin II expression and function in heart development. *Front Biosci (Landmark Ed)* **17**:545-555.
22. Marigo V, *et al.* (2004) Correlation between the clinical phenotype of MYH9-related disease and tissue distribution of class II nonmuscle myosin heavy chains. *Genomics* **83**(6):1125-1133.

23. Phillips HM, Murdoch JN, Chaudhry B, Copp AJ, & Henderson DJ (2005) Vangl2 acts via RhoA signaling to regulate polarized cell movements during development of the proximal outflow tract. *Circ Res* **96**(3):292-299.
24. Han MK & de Rooij J (2016) Converging and Unique Mechanisms of Mechanotransduction at Adhesion Sites. *Trends Cell Biol* **26**(8):612-623.
25. Lowery J, Kuczmarski ER, Herrmann H, & Goldman RD (2015) Intermediate Filaments Play a Pivotal Role in Regulating Cell Architecture and Function. *J Biol Chem* **290**(28):17145-17153.
26. Herrmann H, Bar H, Kreplak L, Strelkov SV, & Aebi U (2007) Intermediate filaments: from cell architecture to nanomechanics. *Nat Rev Mol Cell Biol* **8**(7):562-573.
27. Block J, Schroeder V, Pawelzyk P, Willenbacher N, & Koster S (2015) Physical properties of cytoplasmic intermediate filaments. *Biochim Biophys Acta* **1853**(11 Pt B):3053-3064.
28. Wiche G, Osmanagic-Myers S, & Castañón MJ (2015) Networking and anchoring through plectin: a key to IF functionality and mechanotransduction. *Curr Opin Cell Biol* **32**:21-29.
29. Giancotti FG & Ruoslahti E (1999) Integrin signaling. *Science* **285**(5430):1028-1032.
30. Hynes RO (2002) Integrins: bidirectional, allosteric signaling machines. *Cell* **110**(6):673-687.
31. Bamburg JR (1999) Proteins of the ADF/cofilin family: essential regulators of actin dynamics. *Annu Rev Cell Dev Biol* **15**:185-230.
32. van den Berg G*, et al.* (2009) A caudal proliferating growth center contributes to both poles of the forming heart tube. *Circ Res* **104**(2):179-188.
33. Kelly RG, Buckingham ME, & Moorman AF (2014) Heart Fields and Cardiac Morphogenesis. *Cold Spring Harbor Perspectives in Medicine* **4**(10):a015750.
34. Vitelli F, Huynh T, & Baldini A (2009) Gain of Function of Tbx1 Affects Pharyngeal and Heart Development in the Mouse. *Genesis* **47**(3):188-195.
35. Zhang Z, Huynh T, & Baldini A (2006) Mesodermal expression of Tbx1 is necessary and sufficient for pharyngeal arch and cardiac outflow tract development. *Development* **133**(18):3587-3595.
36. Chen L, Fulcoli FG, Tang S, & Baldini A (2009) Tbx1 regulates proliferation and differentiation of multipotent heart progenitors. *Circ Res* **105**(9):842-851.
37. Tornavaca O*, et al.* (2015) ZO-1 controls endothelial adherens junctions, cell-cell tension, angiogenesis, and barrier formation. *J Cell Biol* **208**(6):821-838.
38. Crawford BD, Henry CA, Clason TA, Becker AL, & Hille MB (2003) Activity and distribution of paxillin, focal adhesion kinase, and cadherin indicate cooperative roles during zebrafish morphogenesis. *Mol Biol Cell* **14**(8):3065-3081.
39. Bazellieres E*, et al.* (2015) Control of cell-cell forces and collective cell dynamics by the intercellular adhesome. *Nat Cell Biol* **17**(4):409-420.
40. le Duc Q*, et al.* (2010) Vinculin potentiates E-cadherin mechanosensing and is recruited to actin-anchored sites within adherens junctions in a myosin II-dependent manner. *J Cell Biol* **189**(7):1107-1115.
41. Yamada S, Pokutta S, Drees F, Weis WI, & Nelson WJ (2005) Deconstructing the cadherin-catenin-actin complex. *Cell* **123**(5):889-901.
42. Barry AK*, et al.* (2014) alpha-catenin cytomechanics--role in cadherin-dependent adhesion and mechanotransduction. *J Cell Sci* **127**(Pt 8):1779-1791.
43. Dorland YL & Huveneers S (2017) Cell-cell junctional mechanotransduction in endothelial remodeling. *Cell Mol Life Sci* **74**(2):279-292.
44. Huveneers S*, et al.* (2012) Vinculin associates with endothelial VE-cadherin junctions to control force-dependent remodeling. *J Cell Biol* **196**(5):641-652.
45. Kano Y, Katoh K, Masuda M, & Fujiwara K (1996) Macromolecular composition of stress fiber-plasma membrane attachment sites in endothelial cells in situ. *Circ Res* **79**(5):1000-1006.
46. Playford MP, Vadali K, Cai X, Burridge K, & Schaller MD (2008) Focal adhesion kinase regulates cell-cell contact formation in epithelial cells via modulation of Rho. *Exp Cell Res* **314**(17):3187-3197.
47. Watabe-Uchida M*, et al.* (1998) alpha-Catenin-vinculin interaction functions to organize the apical junctional complex in epithelial cells. *J Cell Biol* **142**(3):847-857.

48. Gumbiner BM (1996) Cell adhesion: the molecular basis of tissue architecture and morphogenesis. *Cell* **84**(3):345-357.
49. Ma X & Adelstein RS (2014) A point mutation in Myh10 causes major defects in heart development and body wall closure. *Circ Cardiovasc Genet* **7**(3):257-265.
50. Tullio AN, *et al.* (1997) Nonmuscle myosin II-B is required for normal development of the mouse heart. *Proc Natl Acad Sci U S A* **94**(23):12407-12412.
51. Lindsay EA, *et al.* (2001) Tbx1 haploinsufficieny in the DiGeorge syndrome region causes aortic arch defects in mice. *Nature* **410**(6824):97-101.
52. Carpenter AE, *et al.* (2006) CellProfiler: image analysis software for identifying and quantifying cell phenotypes. *Genome Biol* **7**(10):R100.

Table 1: Primary antibodies for western blotting analysis

Paxillin	Mouse	Thermo AHO0492
Paxillin	Rabbit	Abcam ab32084
Paxillin	Rabbit	Santa Cruz sc-5574
E-cadherin	Mouse	BD #610182
Vinculin	Mouse	Sigma #V9131
Pospho-Pxn	Rabbit	Cell Signaling #2541
FAK	Mouse	Santa Cruz #1688
Pospho-FAK (Y925)	Goat	Santa Cruz #sc-11766
Pospho-FAK (Y397)	Rabbit	Cell Signaling #8556
Pospho-ERK (p44/42)	Rabbit	Cell Signaling #9101
ERK	Rabbit	Cell Signaling #9102
Integrin beta1 (cloneMB1.2)	Rat	Millipore MAB1997
TBX1	Rabbit	Abcam #ab18530
Laminin B	Goat	Santa Cruz sc-6216
GAPDH	Mouse	Abcam #125247
Cofilin1	Rabbit	Cell Signaling #3318
Pospho-Cofilin1	Rabbit	Cell Signaling #3311
DDR1	Rabbit	Santa Cruz #sc-532

Table 2: Primary antibodies for immunofluorescence analysis

Paxillin	Rabbit	Abcam ab32084
E-cadherin	Mouse	BD #610182
Integrin β1	Rat	Millipore MAB1997
Active integrin β1 (clone 9EG7)	Rat	BD#550531
Giantin	Rabbit	Abcam #ab24586
Beta-catenin	Mouse	BD #610154
NMII	Rabbit	BioLegend PRB-445P
Vimentin	Mouse	Cell Signaling #3932
Collagen I	Rabbit	Abcam #34710
alpha-tubulin	Mouse	Sigma #T9026
Acetylated tubulin	Mouse	Sigma #T7451

FIGURE LEGENDS

Figure 1. TBX1 regulates cell migration and polarity

(A-B) siRNAs-transfected C2C12 cells (A) or MEF (B) were plated on COLI-coated Transwell filters containing 10% FBS in the bottom well. The migration values are the means ± s.d. of three experiments performed in triplicate, normalized to the number of migrating cells in the absence of FBS, shown as fold change relative to control (*p< 0.05). **(C)** Left panel: phase contrast images taken from a time-lapse series at 16 hours after scratch wounding of control (NT) and *Tbx1*^{KD} cells (scale bar: 100 μm); right panel: Scratch wound area, showed as percentage of the initial wound area as determined using ImageJ software. The values are the means ± s.d. of two independent experiments (*p< 0.05). **(D)** Images of immunofluorescence with anti-Giantin and staining with phalloidin (F-actin) (upper panels) and respective high magnification views (lower panels); arroweads indicate lamellipodia structures. Cells were transfected with the indicated siRNA, and after 42 hrs, a wound was made using a pipette tip and cells were allowed to migrate and polarize for approximately 5 hrs, then they were fixed and processed for immunofluorescence; arrows indicate the Giantin signal. The histogram on the right shows quantification of data: the Giantin signal was counted as oriented towards the wound (polarized cells) if its major mass was located within a 120° angle facing the wound edge (scale bar, 50μm). Results are means ± s.d. from three independent experiments (>300 cells/each). (**E**) Representative pictures of alpha-tubulin immunofluorescence in control (NT) or *Tbx1*^{KD} cell. Arrows and arrowheads indicate leading or trailing edge of the control cell, respectively (scale bar, 25μm).

Figure 2. TBX1 affects cell morphology and cell spreading.

(A) Quantification of cell area (left panel) and cell perimeter (right panel) of siRNAs-transfected C2C12 cells after seeding on plastic uncoated or coated with COLI or FN for 30 min (mean ± s.d from four different experiments with >300 cells per condition). NT: non-targeting control siRNA. Cell area and perimeter were determined by using ImageJ software. Values are shown relative to NT (***p < 0.001; ** p < 0.01). **(B)** Representative phase-contrast images of cells plated on COLI at sparse density for 20 min (top panels) or Phalloidin staining of spread cells after 30 min on COLI (bottom panels); white arrow represents lamella (scale bar, 20μm). **(C)** Flow citometry-based quantification of forward scatter (FSC) and side scatter (SSC) parameters (means ± s.d., n=3). **(D)** Adhesion assay: siRNAs-transfected cells were allowed to adhere to uncoated or ECM-coated wells for 60 min (on plastic, white; on COLI, black and on FN, gray). Values are the means ± s.d. of four independent experiments, each performed in triplicate. **(E)** After 48hrs from siRNAs transfection, C2C12 cells were subjected to RNA extraction for qPCR. Relative RNA levels of ITGB1 were

normalized to Rpl13a expression. Asterisks above bars indicate significant differences compared with controls (***p<0.05). Error bars: s.d.; n=3. **(F)** C2C12 cells were transfected with siRNAs, and stained for surface levels of ITGB1, then analysed by flow cytometry. Values are the mean fluorescence of the population ± s.d. of two separate experiments each performed in duplicate. **(G-H)** Confocal images of siRNAs-treated cells seeded on COLI and stained with anti-PXN and anti-ITGB1 integrin antibodies. Nuclei were stained with DAPI. Arrows indicate FAs (scale bar, 15μm). **(I)** Aberrant cell protrusions in *Tbx1*^{KD} cells seeded on plastic (white columns) or COLI (black columns): photomicrographs (left panel) or quantification (right panel) (scale bar, 50μm). Values are the mean ± s.d. of three experiments (* $p < 0.05$).

Figure 3. TBX1 controls FA formation in C2C12 cells.

(A) After 48hrs from siRNAs transfection, C2C12 cells were subjected to RNA and protein extraction for qPCR (top panel) and western blot (bottom panel) assays, respectively. Top panel: relative RNA levels were normalized to Rpl13a expression. Asterisks above bars indicate significant differences compared with controls (***p<0.001). Error bars: s.d.; n=3. Bottom panel: immunostaining of PXN and GAPDH (loading control). Data are representative of three independent experiments. **(B)** Representative pictures of cells immunostained with PXN (top panels), phosphorylated PXN (P-Pxn Y118) (middle panels) or VCL antibodies (bottom panels). (**C**) Graphs show the quantification of area occupied by FAs, perimeter covered by FA and the number FAs/per cell, relative to the total corresponding spreading values (NT, white columns; *Tbx1*^{KD}, black columns). All quantitative analyses were performed separately, considering FAs positive for anti-PXN (>100 cells), anti-P-PXN (>40 cells) or anti-Vcl (>60 cells). The quantitative analysis was carried out by Cell Profiler software (mean ± s.d. from three different experiments) (scale bars, 25μm). Values are shown relative to NT control cells (*$p < 0.05$; **$p < 0.01$). **(D)** Confocal images of immunofluorescence staining of cells seeded on ECM proteins showing FAs and focal complexes. Nuclei were stained with DAPI. (scale bars: 25μm).

Figure 4. ECM and integrins are alterated in *Tbx1* mutants

(A-B) Transverse sections of E9.5 embryos showing the distribution of COLI in the SpM. Arrows indicate COLI accumulation in the *Tbx1*$^{-/-}$ mutant (scale bar, 100μm). **(C-D)** Confocal images of COLI immunostaining at SHF level of WT (C) and *Tbx1*$^{-/-}$ embryos (D) (sagittal sections, E9.5). In the WT, COLI forms a rudimentary basal lamina while in *Tbx1*$^{-/-}$ embryos its distribution is abnormal, showing an accumulation between eSHF cells (see arrows) (scale bar, 40μm). (**E-F**) ITGB1 immunostaining of E9.5 WT and *Tbx1*$^{-/-}$ embryos. In the WT embryo the signal is present in the anterior SHF and is not detectable in *Tbx1*$^{-/-}$ embryo (see arrows) (scale bar, 20μm). NT, notocord; PE, pharyngeal endoderm; OFT, outflow tract; A, anterior; P, posterior; V, ventral; D, dorsal.

Figure 5. TBX1 regulates FA and cell-adhesion proteins at the eSHF.

(A-B) Immunofluorescence on sagittal sections of E9.5 wild-type (WT) and *Tbx1*$^{-/-}$ embryos, showing the distribution of PXN. (A) In the WT embryo PXN accumulates predominantly at the apical side and cell junctions (arrow), forming a nearly continuous line in the apical membrane of eSHF cells. PXN staining was also found in the basal domain (arrowheads) of eSHF cells. In the endoderm PXN staining marks both apical and basal domains. (B) In the *Tbx1*$^{-/-}$ embryo, the PXN pattern in the eSHF cells is completely abolished (scale bar, 20μm). **(C-D)** Immunostaining of VCL on sagittal sections of a E9.5 WT and *Tbx1*$^{-/-}$ embryos. (C) In the WT embryo, VCL displays an apical domain in the eSHF cells (arrowhead), similarly to the PXN domain. (D) In the *Tbx1*$^{-/-}$ embryo, this characteristic pattern of VCL is severely affected (scale bar, 30μm). OFT, outflow tract; A, anterior; P, posterior; V, ventral; D, dorsal.

Figure 6. Apical-junctional co-localization of PXN and CDH1 in the eSHF.

Immunofluorescence of sagittal sections of E9.5 WT embryos showing the distribution of PXN and the cell-cell junction proteins CHD1 and beta-catenin. PXN accumulates in the apical-lateral domain of eSHF cells and partially overlap with CHD1-positive junctions (see arrow) (A-D), or with beta-catenin-positive junctions (arrows) (E-H) (scale bars, 40μm). High-magnification views are boxed in A and E (scale bar, 10μm). OFT, outflow tract; A, anterior; P, posterior; V, ventral; D, dorsal.

Figure 7. TBX1 is required to maintain actomyosin distribution and cell polarity in the eSHF.

(A-B) Sagittal sections showing F-actin staining. In the WT (A) F-actin is localized at the cell cortex (arrows); in the *Tbx1*$^{-/-}$ embryo (B) the staining is lost in the eSHF. Nuclei were stained with DAPI (scale bar, 10μm). **(C-D)** Confocal images of immunofluorescence of sagittal sections of E9.5 WT and *Tbx1*$^{-/-}$ embryos stained with NMIIB antibody. NMIIB is apically distributed in WT embryos (arrows) while in the *Tbx1*$^{-/-}$ embryo the protein surrounds the entire perimeter of the cells (arrows) (scale bar, 40μm). **(E-F)** Immunofluorescence images of sagittal sections of E9.5 WT and *Tbx1*$^{-/-}$ embryos by using a Giantin antibody. (E) In the WT embryo, Giantin is oriented towards the pericardial cavity as its major mass was located within a 120° angle facing the apical membrane (arrow). (F) In the *Tbx1*$^{-/-}$ embryo embryo it is localised mostly laterally to the cells (arrow) (scale bar, 20μm). **(G)** Quantitative analysis of Giantin polarization data. Histograms show the mean ± s.d. of >100 cells in 3 embryos. Values are shown relative to control ($*p < 0.05$). (H-I) In the WT embryo, VIM-positive cells are very rare. In the *Tbx1*$^{-/-}$ embryo the number of SHF cells stained with VIM is strongly increased (scale bar, 40μm). A, anterior; P, posterior; V, ventral; D, dorsal.

Figure 8. *Tbx1*-depleted cells fail to respond to ECM-FAs signalling.

(A) After 48hrs from siRNAs transfection, C2C12 cells were plated on COLI or FN and lysed after 20 min. Cell lysates were analysed by immunoblotting with antibodies to the indicated phosphorylated and to total protein levels of the respective protein. P-PXN, P-FAK and P-ERK1/2 levels were normalised to total PXN, FAK and ERK1/2 levels, respectively. GAPDH was used as a loading control. (**B**) Histograms show densitometric analysis of immunoblots. Values are levels of the normalized phosphorylated proteins relative to those in control cells (NT) (n=3 for each protein; means ± s.d. *p<0.05, ** p<0.01 versus control).

Figure 9. TBX1 regulates NMIIB and VIM distribution in the SHF in a cell non autonomous manner

(**A-B**) Timed fate mapping of *Tbx1* in E9.5 *Tbx1*$^{mcm/+}$; *R26R* embryos exposed to TM at E7.5, stained with NMIIB (green) and GFP (red) antibodies. GFP+ *Tbx1* homozygous cells (A-A') and GFP+ *Tbx1* heterozygous cells (B-B') show identical apical NMIIB localization (arrows) (scale bars, 20μm). The regions shown in A and in B are boxed in A' and B', respectively (scale bars, 10μm). Single channels of this picture are shown in Supplementary Fig.7A **(C-D)** Timed fate mapping of *Tbx1*-expressing cells in E9.5 *Tbx1*$^{mcm/+}$; *R26R* embryos exposed to TM at E7.5, stained with GFP (green), CDH1 (red) and VIM (white) antibodies. GFP+ *Tbx1* homozygous cells (C) and GFP+ *Tbx1* heterozygous cells (D) show similar CDH1 and VIM staining (arrows) (scale bars, 20μm) Single channels of this picture are shown in Supplementary Fig.7B OFT, outflow tract; A, anterior; P, posterior; V, ventral; D, dorsal.

Figure 10. Cartoon showing a model of TBX1 function in the eSHF.

Supplementary Figure legends

Supplementary Figure 1. Effects of Tbx1 knockdown.

(A) To confirm *Tbx1* knockdown efficiency, at indicated times from siRNAs transfection, C2C12 cells were subjected to western blot analysis by using anti-TBX1 antibody. Lamin B was used as a loading control. **(B)** After 24h from siRNAs transfection, C2C12 cells were maintained in culture for 16hrs, 24hrs or 48hrs and then subjected to proliferation assay measured by the CyQuant assay. Values are expressed as relative to control NT. Values are the means ± s.d. of three experiments performed in triplicate (*p< 0.05).

Supplementary Figure 2. Actin protrusions and microtubule arrangements in *Tbx1*-depleted C2C12 cells.

(A) Quantitaive analysis of membrane lamellipodial protrusions in the migrating C2C12 cell sheet, measured by two different parameters: Lamellipodial density or number of cell protruding facing wound margin. Values are the means ± s.d. of two independent experiments (*p< 0.05).

(B) Representative pictures of microtubules immunostained with alpha-tubulin (right panels) or anti-acetylated-tubulin (left panels). In all images PXN is shown in green. (scale bar, 15μm).

Supplementary Figure 3. COL1 and ITGB1 immunofluorescence.

Transverse sections of E9.5 embryos showing the distribution of COLI (green) and ITGB1 (red) at the SHF level in WT (A) and *Tbx1*$^{-/-}$ embryos (B). (scale bar, 100μm). PE, pharyngeal endoderm; DPW dorsal pericardial wall.

Supplementary Figure 4. ITGB1 and COLI localization at the SHF.

(A) Immunofluorescence of sagittal sections of E9.5 WT embryos showing the distribution of ITGB1 and COLI. At basal side of eSHF cells is shown a partial colocalization between the two proteins (scale bar, 30 μm). OFT, outflow tract; A, anterior; P, posterior; V, ventral; D, dorsal.

Supplementary Figure 5. CDH1 is altered in *Tbx1* mutants.

(A-B) In a WT embryo, CHD1 is observed on the apical-lateral domains of the eSHF monolayer, predominantly in the anterior region of the SHF (arrows). In the *Tbx1*$^{-/-}$ embryo, the CHD1 signal is reduced or completely abolished in the posterior-lateral regions of SHF (scale bar, 15μm). A, anterior; P, posterior; V, ventral; D, dorsal.

Supplementary Figure 6. VIM expression is increased in the SHF of *Tbx1*$^{-/-}$ embryos.

Transverse sections at E9.5 showing the distribution of VIM (green) in WT (A) and *Tbx1*$^{-/-}$ embryos (B); arrows indicate the increased levels of VIM in *Tbx1* mutant at SHF level (scale bar, 20μm). PE, pharyngeal endoderm; DPW dorsal pericardial wall.

Supplementary Figure 7. VIM expression is increased in the SpM of *Tbx1*$^{-/-}$ embryos.
Transverse sections at E9.5 showing the distribution of VIM (green) in SpM of WT (A-B) and *Tbx1*$^{-/-}$ embryos (C-D); arrows indicate the increased levels of VIM in *Tbx1* mutant at SpM level (scale bar, 50μm). PE, pharyngeal endoderm; NT, notocorde.

Supplementary Figure 8. *TBX1* regulates FA signalling in an ECM-dependent manner.

(A) After 48hrs from siRNAs transfection, C2C12 cells were plated on COLI or FN and lysed after 20 min. Cell lysates were analysed by immunoblotting with Pospho-CFL1 antibody. The levels were normalised to total CFL1. GAPDH was used as a loading control. **(B)** After 48 hrs from siRNAs transfection, C2C12 cells were plated on COLI or FN and lysed after 20 min. Cell lysates were analysed by immunoblotting with antibodies to the indicated phosphorylated proteins. GAPDH was used as loading control. *Pxn*-depleted cells were used as positive controls of the experiment.

Supplementary Figure 9. TBX1 is required to maintain morphogenetic properties of SHF in a cell non autonomous manner

(**A**) Timed fate mapping of *Tbx1*-expressing cells in E9.5 *Tbx1*$^{mcm/+}$; *R26R* embryos exposed to TM at E7.5, stained with GFP (red), NMIIB (green) and CDH1 (white) (scale bar, 20 μm) or **(B)** with GFP (green), CDH1 (red) and VIM (white) antibodies (scale bar, 20 μm). DAPI was used for staining of nuclei. GFP+ *Tbx1* homozygous cells (arrows) show similar NMIIB, CDH1 and VIM staining compared to surrounding heterozygous cells of the same embryo (arrows). The panels showing the merged images are also exhibited in Fig.9. OFT, outflow tract; A, anterior; P, posterior; V, ventral; D, dorsal.

Supplementary Movie 1 and Movie2.

3D reconstructions of PXN (green) and CDH1 (red) in outer layer of SHF by Nikon A1 confocal software.

Figure 1

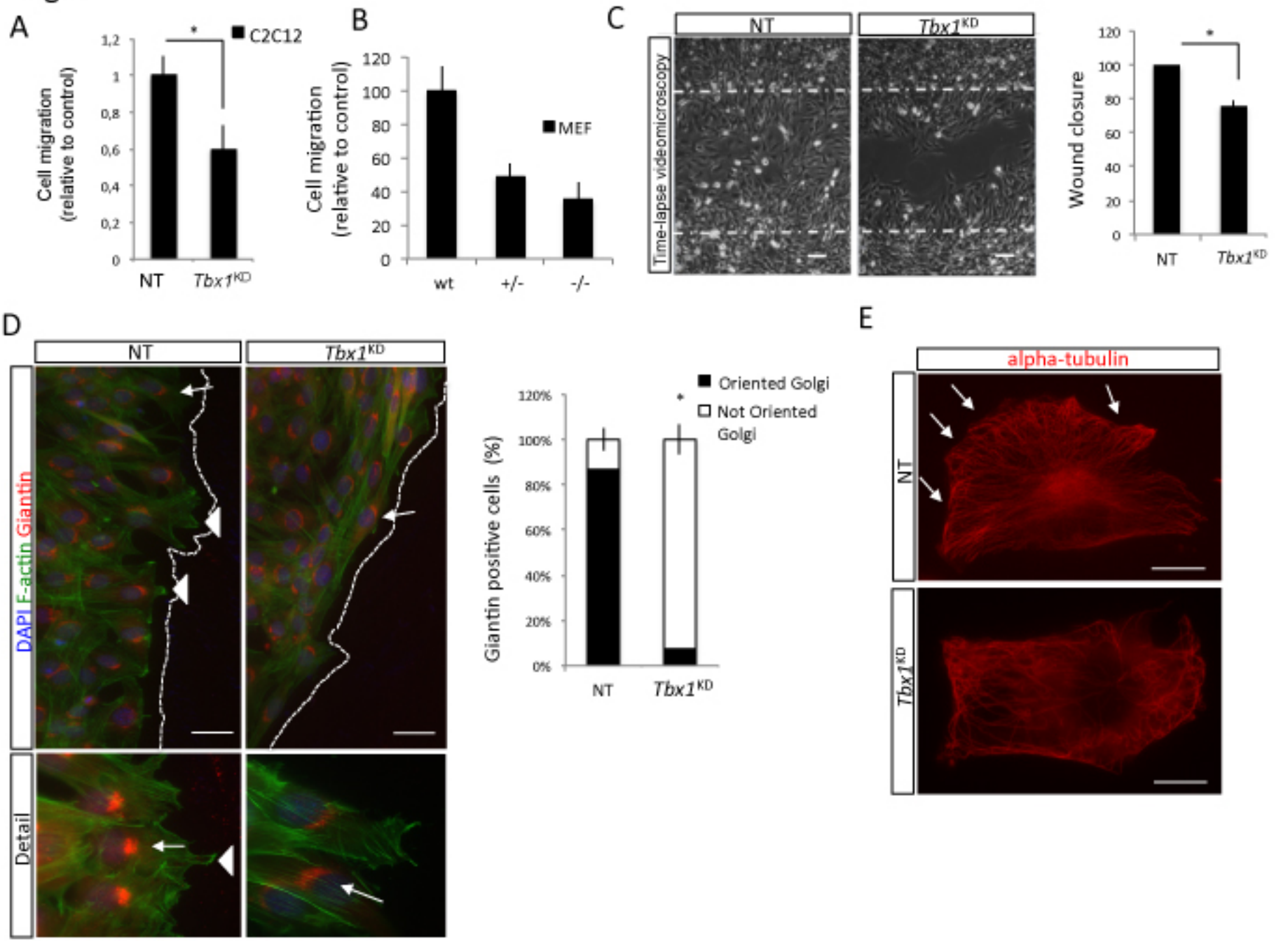
A
C2C12
Cell migration (relative to control)
1,2
1
0,8
0,6
0,4
0,2
0
*
NT
Tbx1KD
B
MEF
Cell migration (relative to control)
120
100
80
60
40
20
0
wt
+/-
-/-
C
NT
Tbx1KD
Time-lapse videomicroscopy
Wound closure
120
100
80
60
40
20
0
*
NT
Tbx1KD
D
NT
Tbx1KD
DAPI F-actin Giantin
Detail
Oriented Golgi
Not Oriented Golgi
Giantin positive cells (%)
120%
100%
80%
60%
40%
20%
0%
*
NT
Tbx1KD
E
alpha-tubulin
NT
Tbx1KD

Figure 2

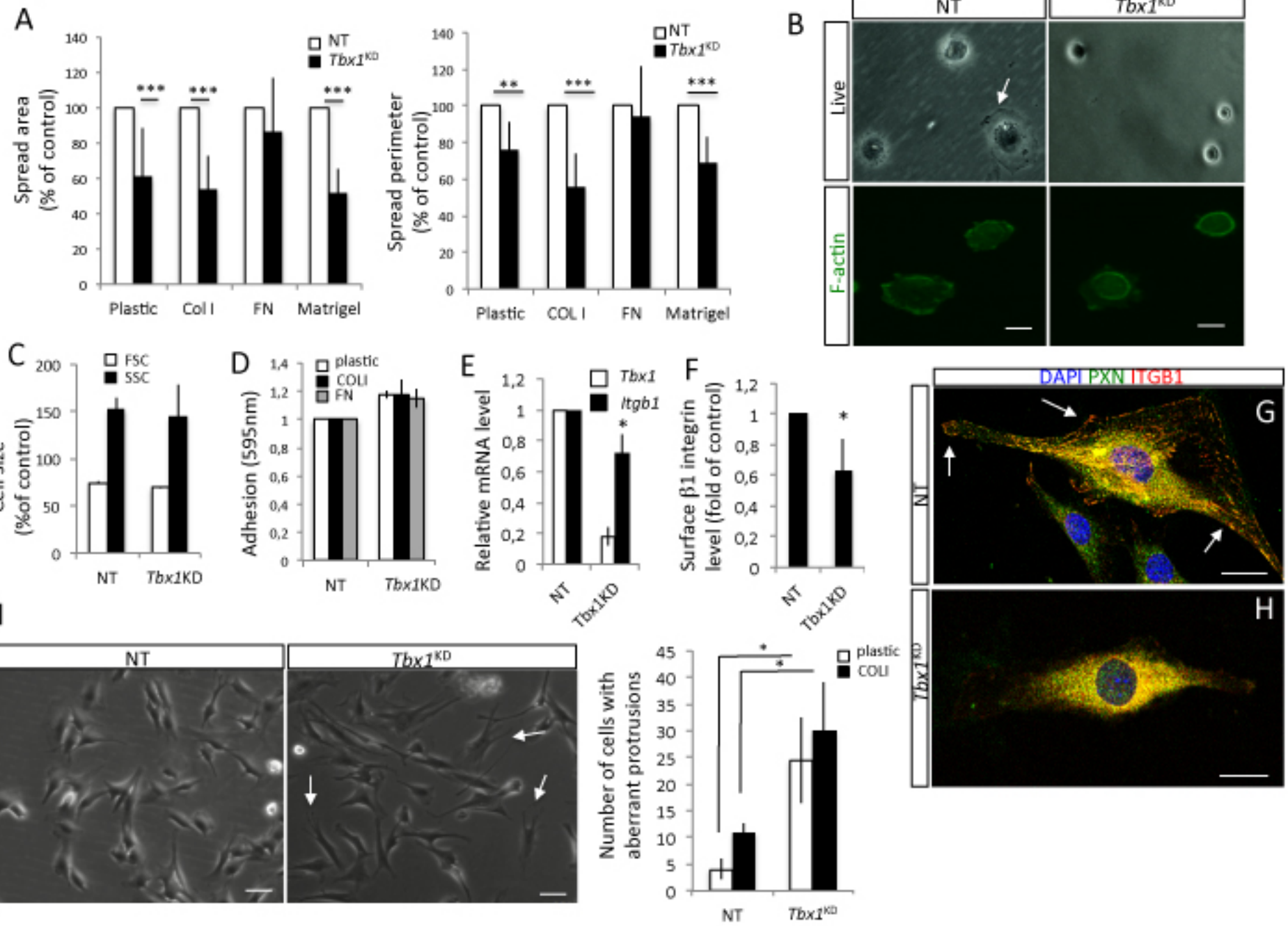
A
Spread area (% of control)
NT
Tbx1KD
Plastic
Col I
FN
Matrigel
Spread perimeter (% of control)
COL I
B
NT
Tbx1KD
Live
F-actin
C
Cell size (%of control)
FSC
SSC
NT
Tbx1KD
D
Adhesion (595nm)
plastic
COLI
FN
E
Relative mRNA level
Tbx1
Itgb1
F
Surface β1 integrin level (fold of control)
DAPI PXN ITGB1
G
H
I
Number of cells with aberrant protrusions
plastic
COLI

Figure 3

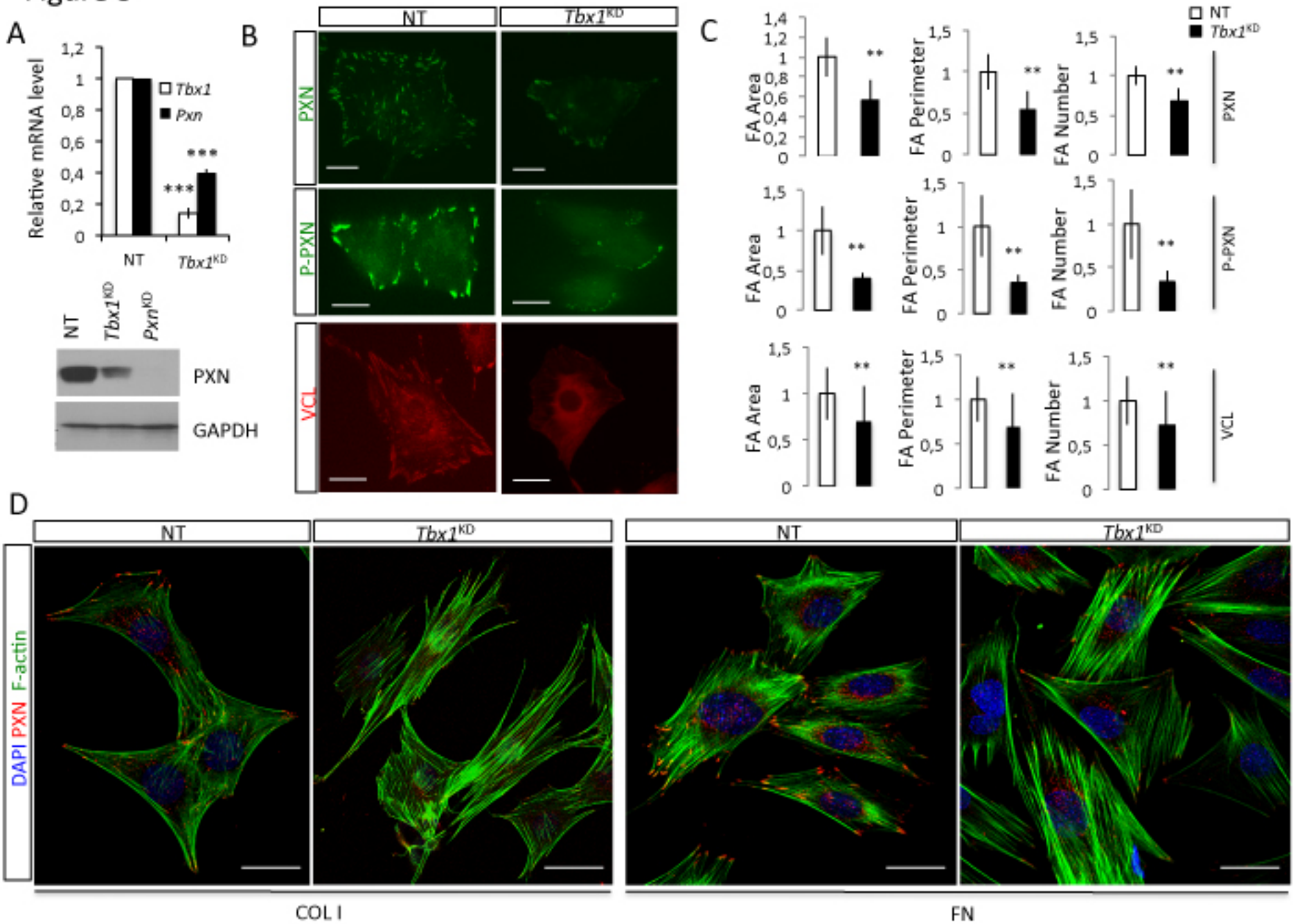
A
Relative mRNA level
1,2
1
0,8
0,6
0,4
0,2
0
Tbx1
Pxn
***
***
NT
Tbx1KD
NT
Tbx1KD
PxnKD
PXN
GAPDH
B
NT
Tbx1KD
PXN
P-PXN
VCL
C
NT
Tbx1KD
FA Area
FA Perimeter
FA Number
PXN
P-PXN
VCL
**
D
NT
Tbx1KD
NT
Tbx1KD
DAPI PXN F-actin
COL I
FN

Figure 4

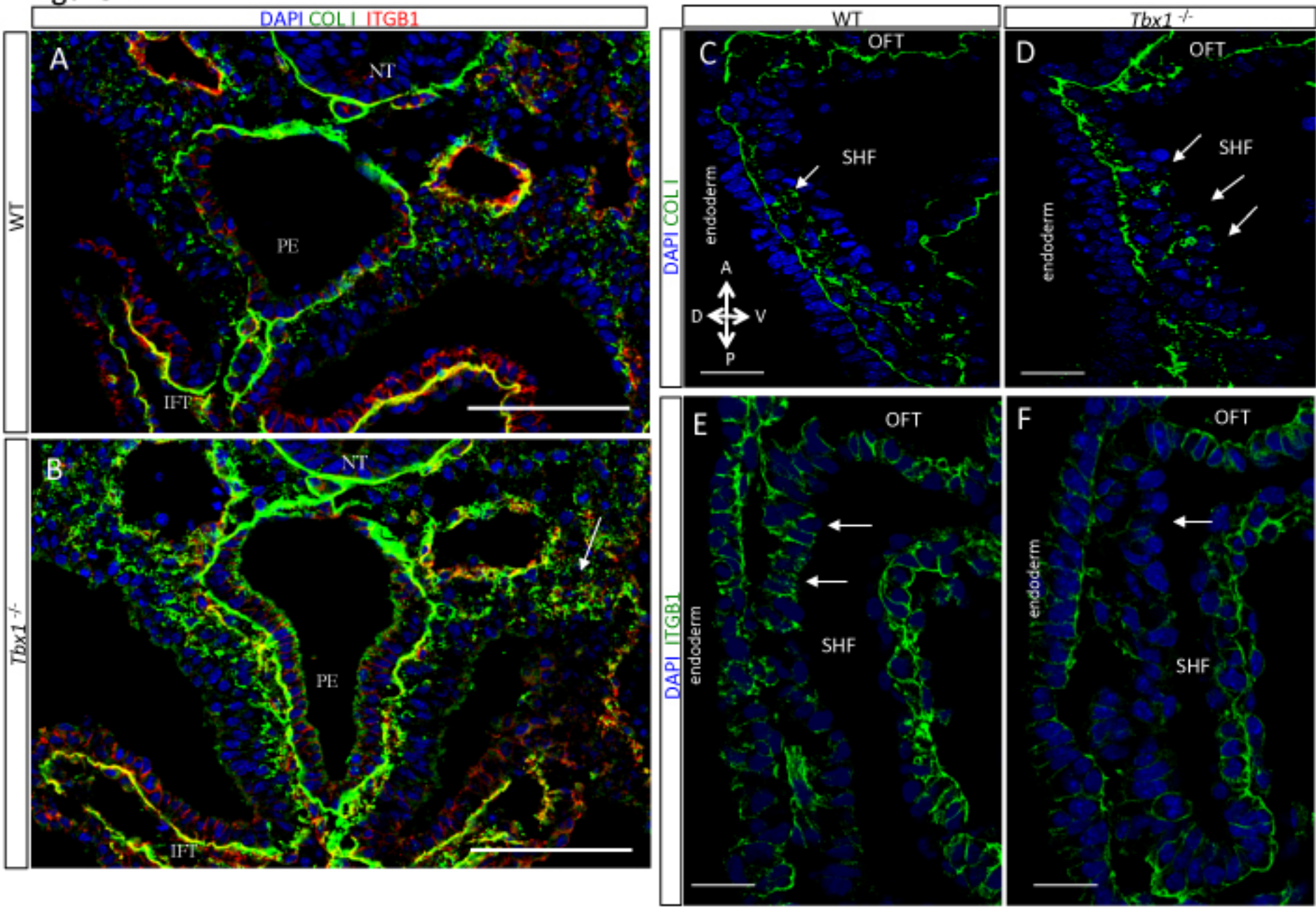
DAPI COL I ITGB1
WT
A
NT
PE
IFT
Tbx1 -/-
B
NT
PE
IFT
WT
Tbx1 -/-
C
OFT
SHF
endoderm
DAPI COL I
A
D
V
P
D
OFT
SHF
endoderm
E
OFT
SHF
endoderm
DAPI ITGB1
F
OFT
SHF
endoderm

Figure 5

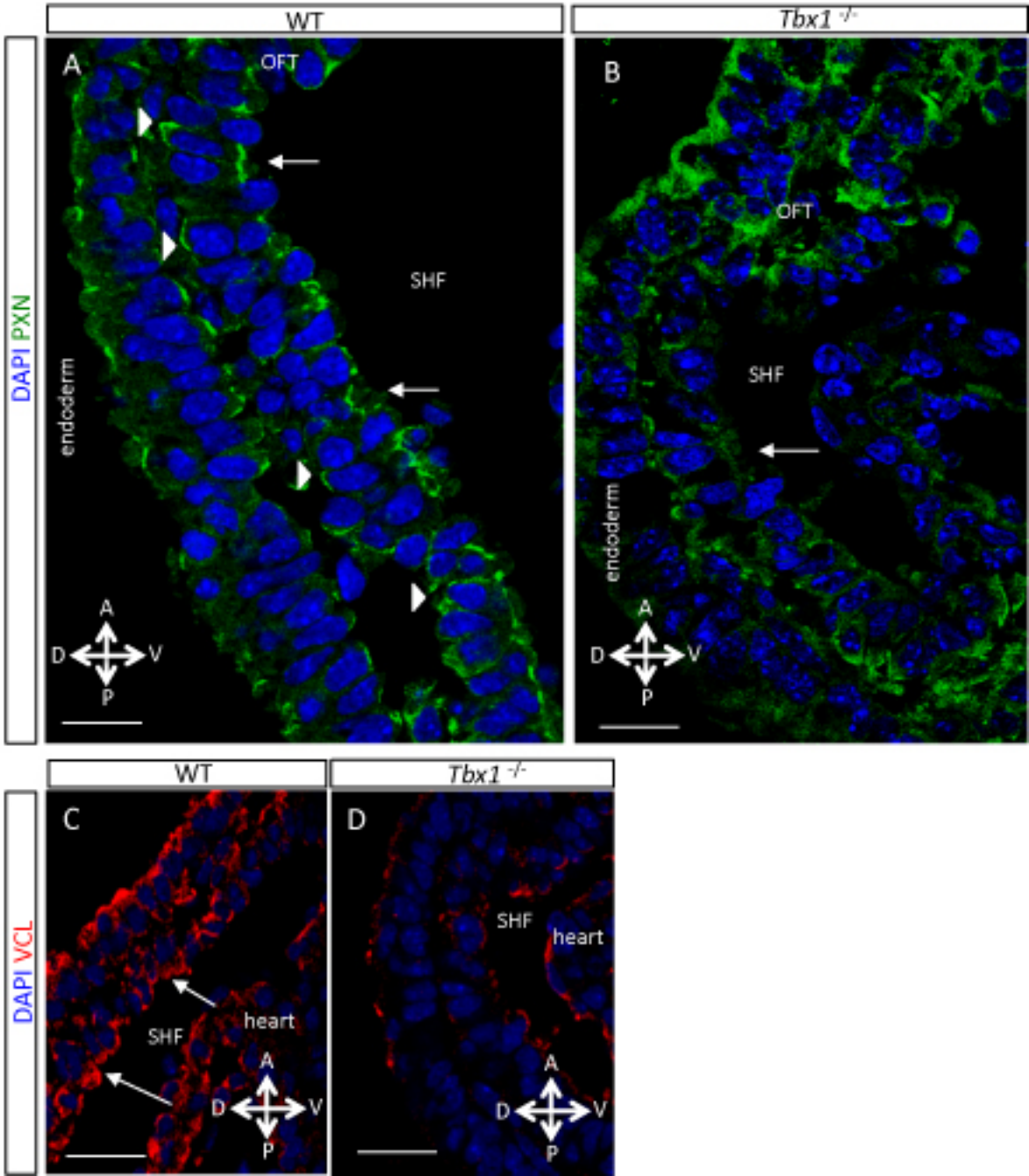
WT
Tbx1 -/-
A
OFT
SHF
endoderm
DAPI PXN
A
D
V
P
B
OFT
SHF
endoderm
A
D
V
P
WT
Tbx1 -/-
C
SHF
heart
DAPI VCL
A
D
V
P
D
SHF
heart
A
D
V
P

Figure 6

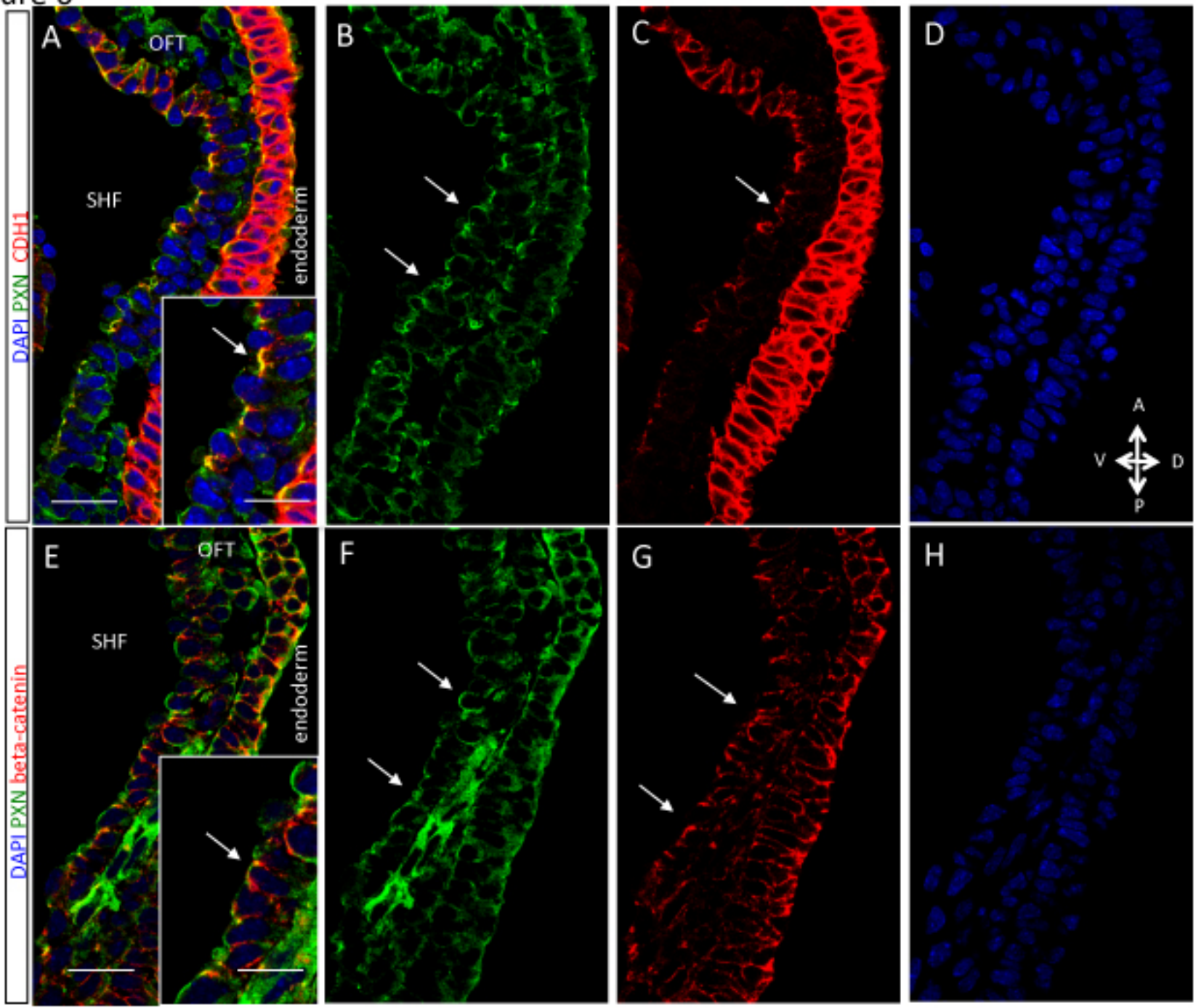
A
OFT
SHF
endoderm
DAPI PXN CDH1
B
C
D
A
V
D
P
E
OFT
SHF
endoderm
DAPI PXN beta-catenin
F
G
H

Figure 7

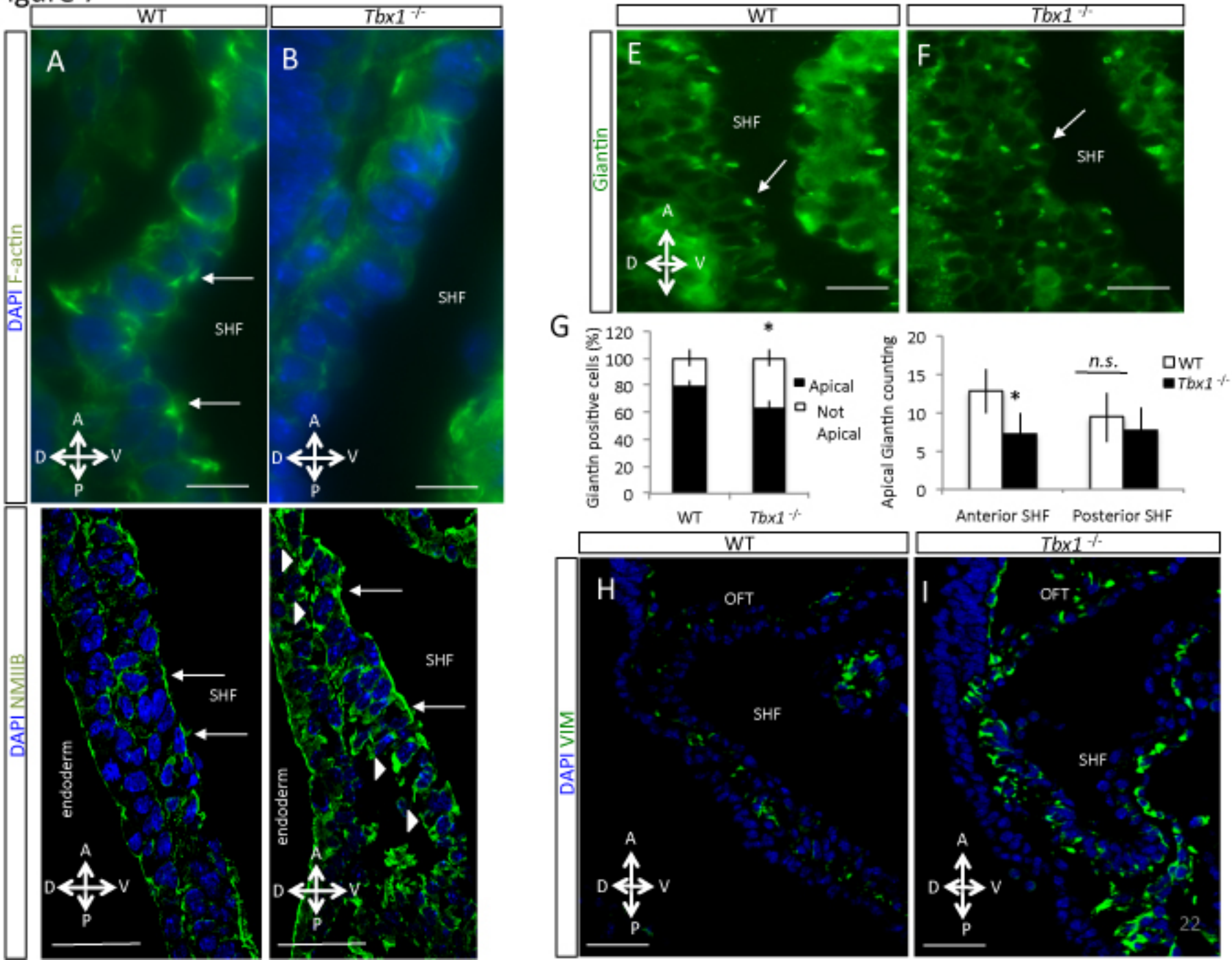
WT
Tbx1 -/-
A
B
DAPI F-actin
SHF
A
D
V
P
endoderm
DAPI NMIIB
E
F
Giantin
G
Giantin positive cells (%)
120
100
80
60
40
20
0
*
Apical
Not Apical
WT
Tbx1 -/-
Apical Giantin counting
20
15
10
5
0
n.s.
Anterior SHF
Posterior SHF
H
I
OFT
DAPI VIM
22

Figure 8

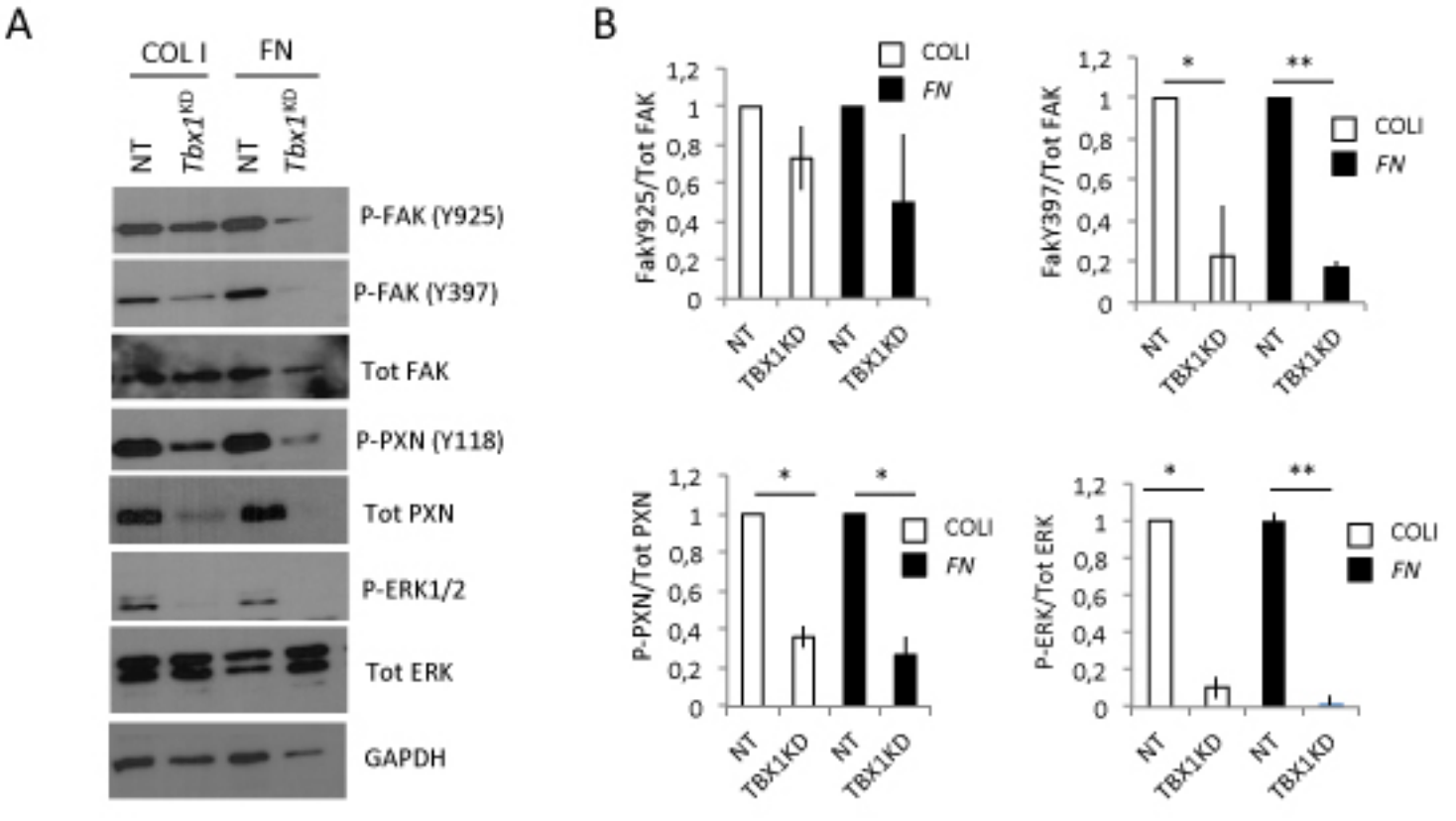
A
COL I
FN
NT
Tbx1KD
NT
Tbx1KD
P-FAK (Y925)
P-FAK (Y397)
Tot FAK
P-PXN (Y118)
Tot PXN
P-ERK1/2
Tot ERK
GAPDH
B
COLI
FN
FakY925/Tot FAK
FakY397/Tot FAK
P-PXN/Tot PXN
P-ERK/Tot ERK
1,2
1
0,8
0,6
0,4
0,2
0
NT
TBX1KD
*
**

Figure 9

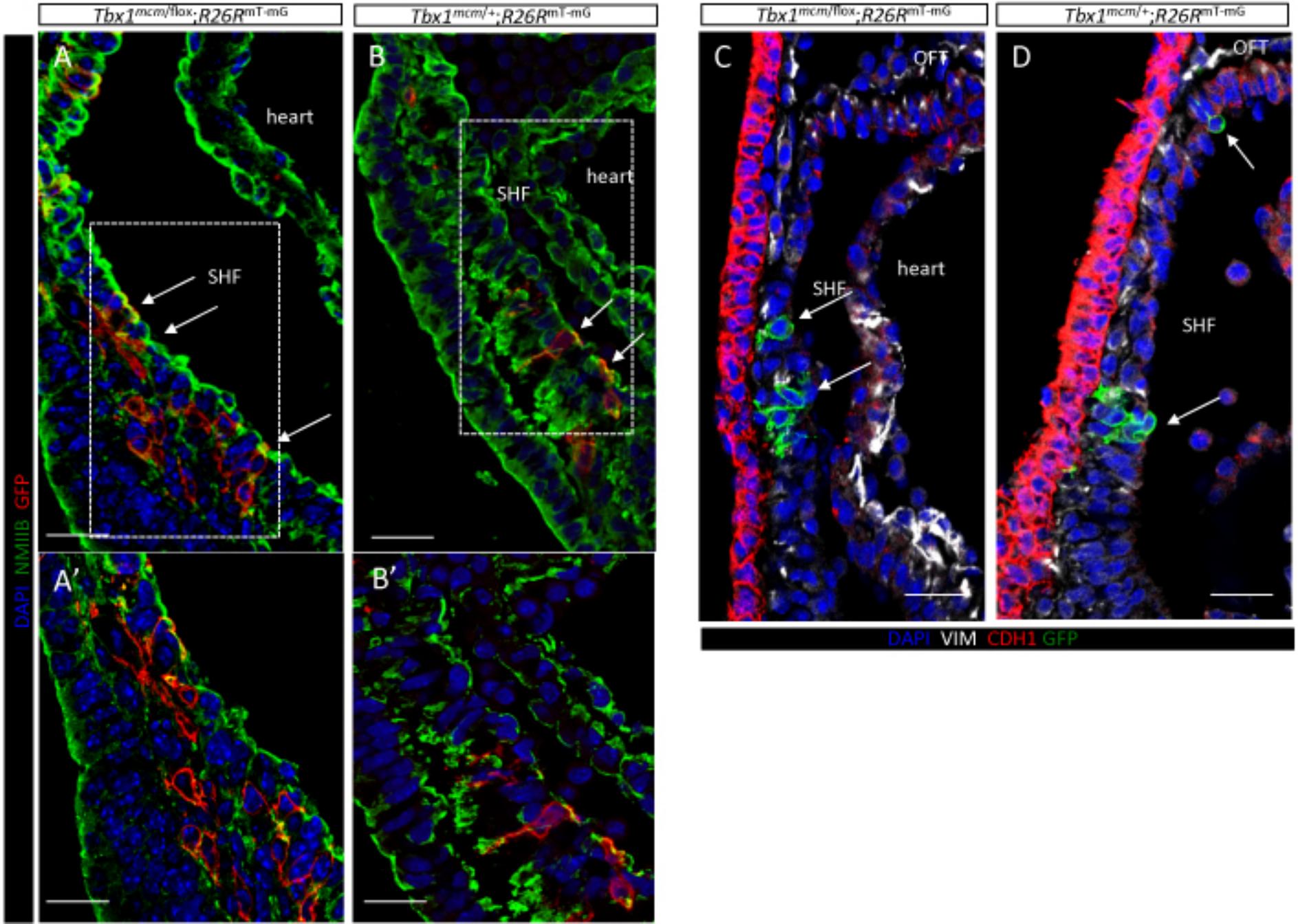
Tbx1mcm/flox;R26RmT-mG
Tbx1mcm/+;R26RmT-mG
Tbx1mcm/flox;R26RmT-mG
Tbx1mcm/+;R26RmT-mG
A
B
C
D
A'
B'
heart
SHF
OFT
DAPI NMIIB GFP
DAPI VIM CDH1 GFP

Figure 10

Schematic summary of TBX1 function in SHF cytoarchitecture and OFT morphogenesis contribution